

# Cluster Magnetic Fields from Galactic Outflows

J. Donnert<sup>1\*</sup>, K. Dolag<sup>1</sup>, H. Lesch<sup>2</sup> and E. Müller<sup>1</sup>

<sup>1</sup>Max Planck Institute for Astrophysics, P.O. Box 1317, D-85741 Garching, Germany

<sup>2</sup>Universitäts-Sternwarte München, Scheinerstr. 1, D-81679 München, Germany

Accepted 2008 October 22. Received 2008 October 13; in original form 2008 August 6

## ABSTRACT

We performed cosmological, magneto-hydrodynamical simulations to follow the evolution of magnetic fields in galaxy clusters, exploring the possibility that the origin of the magnetic seed fields are galactic outflows during the star-burst phase of galactic evolution. To do this we coupled a semi-analytical model for magnetized galactic winds as suggested by Bertone et al. (2006) to our cosmological simulation. We find that the strength and structure of magnetic fields observed in galaxy clusters are well reproduced for a wide range of model parameters for the magnetized, galactic winds and do only weakly depend on the exact magnetic structure within the assumed galactic outflows. Although the evolution of a primordial magnetic seed field shows no significant differences to that of galaxy clusters fields from previous studies, we find that the magnetic field pollution in the diffuse medium within filaments is below the level predicted by scenarios with pure primordial magnetic seed field. We therefore conclude that magnetized galactic outflows and their subsequent evolution within the intra-cluster medium can fully account for the observed magnetic fields in galaxy clusters. Our findings also suggest that measuring cosmological magnetic fields in low-density environments such as filaments is much more useful than observing cluster magnetic fields to infer their possible origin.

**Key words:** (magnetohydrodynamics)MHD - magnetic fields - methods: numerical - galaxies: clusters

## 1 INTRODUCTION

Magnetic fields have been detected in galaxy clusters by radio observations, via the Faraday rotation signal of the magnetized cluster atmosphere towards polarized radio sources in or behind clusters (Carilli & Taylor 2002) and from diffuse synchrotron emission of the cluster atmosphere (see Govoni & Feretti 2004; Ferrari et al. 2008, for recent reviews). However, our understanding of their origin is still very limited.

At present, models for the origin of seed fields can be classified in three main groups. In the first, a magnetic field is created in shocks through the "Biermann battery" effect (Kulsrud et al. 1997; Ryu et al. 1998; Miniati et al. 2001). A subsequent turbulent dynamo boosts it to the field strength observed in galaxy clusters. A second class of models invokes processes that took place in the early universe. In general, they predict that magnetic seed fields fill the entire volume of the universe; however the coherence length of the field crucially depends on the details of the models (see Grasso & Rubinstein 2001, for a review). Finally, galactic winds (e.g. Völk & Atoyan 2000) or AGN ejecta (e.g. Enßlin et al. 1997; Furlanetto & Loeb 2001, and references therein) can produce magnetic fields and pollute the proto-cluster region. In such models, the magnetic field can also originate from an early population of dwarf,

starburst galaxies (Kronberg et al. 1999) at relatively high redshift ( $z \approx 4 - 6$ ).

In previous work, non radiative simulations of galaxy clusters within a cosmological environment which follow the evolution of a primordial magnetic seed field were performed using Smooth-Particle-Hydrodynamics (SPH) codes (Dolag et al. 1999, 2002, 2005) as well as Adaptive Mesh Refinement (AMR) codes (Brüggen et al. 2005; Dubois & Teyssier 2008; Li et al. 2008). Although these simulations are based on different numerical techniques they show good agreement in the predicted properties of the magnetic fields in galaxy clusters, when the evolution of an initial magnetic seed field is followed. This work has also demonstrated, that the properties of the final magnetic field in galaxy clusters do not depend on the detailed structure of the assumed initial magnetic field. The spatial distribution and the structure of the predicted magnetic field in galaxy clusters is primarily determined by the dynamics of the velocity field imprinted by cluster formation (Dolag et al. 1999, 2002) and compares well with measurements of Faraday rotation.

The creation of magnetic fields in shocks through the "Biermann battery effect" (Kulsrud et al. 1997; Ryu et al. 1998), and subsequent turbulent dynamo action can be followed as well as a prediction can be made for magnetic field values from velocity fields inferred in cosmological simulations (Ryu et al. 2008). Both methods predict magnetic field strengths in filaments with some-

\* jdonnert@mpa-garching.mpg.de

what higher values (e.g. see Sigl et al. 2004) than found in simulations that follow the evolution of a primordial magnetic seed field.

Faraday rotation can be observed in several radio galaxies located at different radial distances with respect to the cluster center. Motivated by numerical simulations (Dolag et al. 2001), the observed magnetic field is often modelled with a radially-declining field strength and a power law spectral structure. From such observations, one can constrain the power law spectral index (Murgia et al. 2004; Govoni et al. 2006) or directly reconstruct the power spectrum of the magnetic field (Vogt & Enßlin 2003, 2005). Given the sparse observational data available at the moment, a degeneracy exists between the central value of the magnetic field and its rate of radial decline (see for example Bonafede et al. 2008; Guidetti et al. 2008), for which detailed predictions from simulations can be useful in breaking the degeneracy. The simulations must therefore examine different possible magnetic field origins in galaxy clusters in order to test the robustness of the inferred magnetic field properties.

Recently the validity of models that produce a cluster magnetic field from galactic winds has been supported by a semi-analytic modelling of galactic winds (Bertone et al. 2006). However, these models are unable to predict how the magnetic fields produced by the ejecta of the galaxies are compressed and amplified by the process of structure formation. Therefore, the structure of the final magnetic field in galaxy clusters cannot yet be predicted by these models. In this work we extend these studies by directly incorporating the galactic outflow model in magneto-hydrodynamical simulations of structure formation.

The paper is structured as follows: In section 2 we present the details of the cosmological setup, concentrating especially on the coupling of the semi-analytic model to the cosmological simulations. Details of the wind model and the seed magnetic field are presented in section 3.1 and appendix A. The general results of our simulations are presented in section 4 and in section 5 we discuss our findings, particularly how galaxy clusters formed in our simulations. Finally, we present our conclusions in section 6.

## 2 SIMULATION SETUP

To investigate the evolution of a magnetic seed field produced by galactic outflows one needs to couple the galaxies formed in a cosmological, magneto-hydrodynamical simulation with a model for the galactic outflows.

### 2.1 Initial conditions

We used a constrained realization of the local universe (see Dolag et al. 2005, and references therein), with initial conditions similar to those used by Mathis et al. (2002) in their study of structure formation in the Local Universe. The initial density fluctuations were constructed from the IRAS 1.2-Jy galaxy survey by smoothing the observed galaxy density field on a scale of 7 Mpc, evolving it linearly back in time, and then using it as a Gaussian constraint (Hoffman & Ribak 1991) for an otherwise random realization of the  $\Lambda$ CDM cosmology. The volume constrained by the IRAS observations covers a sphere of radius  $\sim 115$  Mpc centered on the Milky Way. This region is sampled with high resolution dark matter particles and is embedded in a periodic box of  $\sim 343$  Mpc length.

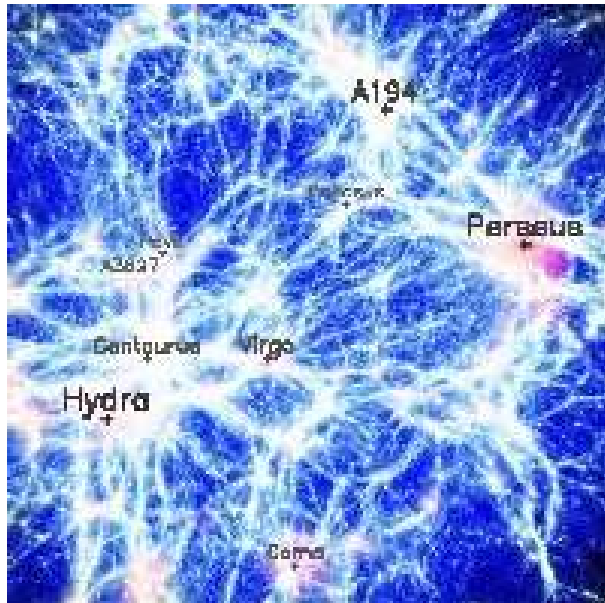


**Figure 1.** Shown is a visualization of the constrained local universe simulation at redshift  $z = 0$  using SPLOTCH (Dolag et al. 2008). Structures which can be identified with their counterparts in the real universe are labelled. An animation flying through the simulation can be downloaded from the MPA Website <sup>2</sup>.

The gravitational softening length used is  $\epsilon = 14$  kpc, which corresponds to the smallest SPH smoothing length reached in the dense centers of halos. In low density regions, the resolution is lower. The region outside the constrained volume is filled with dark matter particles at lower resolution, allowing a good coverage of long range gravitational tidal forces. Many of the most prominent clusters observed locally can therefore be identified directly with halos in the simulation, and their positions and masses agree well with their simulated counterparts. Figure 1 shows a rendering of the simulation at redshift  $z = 0$  where some of the identified structures are labelled.

In this work we use extended initial conditions where the original high resolution dark matter particles are split into gas and dark matter particles with masses of  $0.69 \times 10^9 M_{\odot}$  and  $4.4 \times 10^9 M_{\odot}$  respectively. The most massive clusters in our simulations are hence resolved by nearly one million particles. The gravitational force resolution (i.e. the gravitational softening length) of the simulations was set to be 14 kpc, which is comparable to the inter-particle separation of the SPH particles in the dense centers of our simulated galaxy clusters.

### 2.2 Seeding strategy

In principal one would like to follow the dynamics of galactic outflows driven by stellar activity (either star-formation or star-burst) self-consistently in cosmological simulations. However, so far this is not possible. Although cooling and star-formation processes can be followed in standard cosmological simulations, the detailed interaction with magnetic fields leads to regions in which the magnetic field pressure exceeds the thermal one, especially in high resolution studies like those we plan to perform. In absence of any dissipative process when performing ideal MHD simulations, these regions then dominate the time-stepping in the simulations and cause them to stall. We therefore took a simpler approach by coupling

<sup>2</sup> [http://www.mpa-garching.mpg.de/galform/data\\_vis/index.shtml#movie12](http://www.mpa-garching.mpg.de/galform/data_vis/index.shtml#movie12)

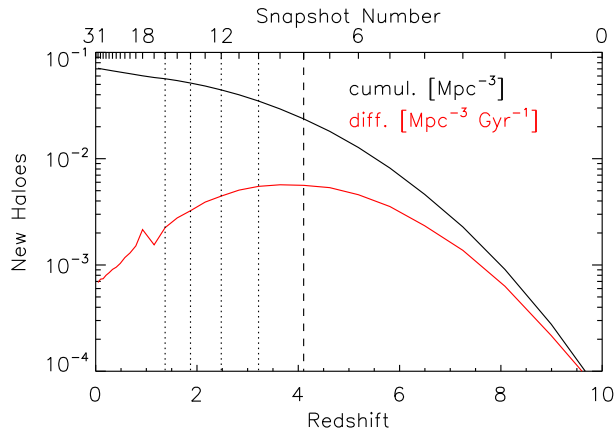


**Figure 2.** Newly formed haloes per Mpc cubed as a function of redshift in the reference simulation, involving a primordial magnetic seed (Dolag et al. 2005). The black curve shows the cumulative distribution, the red curve the differential one (per Gyr). The dashed line marks the time selected for the single seeding, the dotted line marks the additional seeding times in the multi-seed run.

a semi-analytical recipe for star-burst-driven, magnetized outflows (Bertone et al. 2006) with non-radiative, cosmological MHD simulations. In general, this should be implemented as a continuous process, starting at very high redshift  $z \approx 10$  (Kronberg et al. 1999). For practical reasons, we approximate this process by an instantaneous magnetization of all galaxies inferred in the simulations at a selected instance in time (e.g.  $z = 4.1$ ), and then evolve the simulation with magnetic seed fields until the present day. As the cosmological simulation evolves, the magnetized gas is stripped from its host galaxies as it falls towards the dense gas contained in galaxy clusters. The intra cluster medium (ICM) is thereby enriched by the stripped, magnetized gas of several hundreds of galaxies. Furthermore, the magnetized gas is processed by shear-flows and turbulence within the cluster atmosphere, which eventually leads to the magnetic field strength and structure observed today in galaxy clusters. To justify our approximation we also performed one simulation where we repeated the seeding process several times and demonstrated that for cluster magnetic fields these further seedings are irrelevant, as they mainly involve newly-formed galaxies outside the proto-cluster region. The redshift  $z = 4.1$  of the single seeding event was chosen as a compromise between complete formation of all relevant galaxies (e.g. choosing a low seeding redshift) and avoidance of galaxy mergers or destruction in proto-clusters (e.g. choosing a high seeding redshift). Figure 2 shows the number density of formed halos as a function of redshift (differential per Gyr and cumulative) as inferred from our reference run with a cosmological seed field (Dolag et al. 2005). The dashed line marks the preferred redshift of seeding which is chosen to ensure that most of the galaxies in the proto-cluster region are formed and not yet merged with others, destroyed or stripped from their hot gas haloes in the proto-cluster. The dotted line marks the additional seeding times used in the multi-seed reference run. As seeding targets we choose galaxies which are newly formed (i.e. since the last seeding) and whose mass is smaller than  $M_{\text{Halo}} = 3 \times 10^{12} M_{\odot}$  since our wind model does not apply for group like objects. Note that the constraint on mass is only of relevance for the low redshift seeding in the multi-seed reference run.

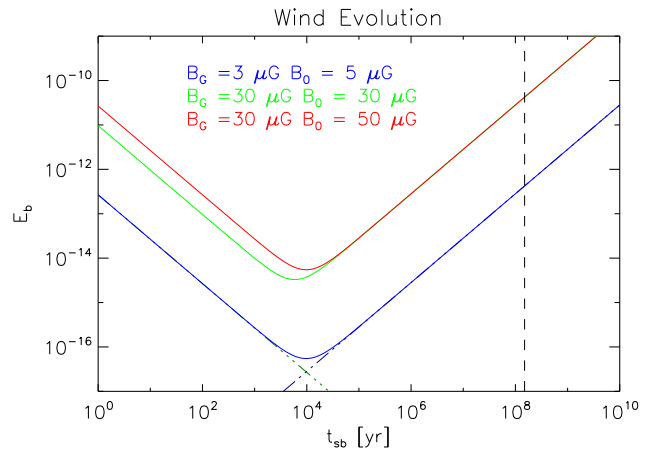


**Figure 3.** Evolution of the magnetic energy in a wind bubble of a small galaxy ( $M_{\text{ISM}} = 10 \times 10^{12} M_{\odot}$ ) for different disc and halo parameters ( $B_G, B_0$ ). The dashed line marks the star-burst time of 150 Myr (de Grijs 2001), the dot-dashed lines mark the envelopes of the two wind phases. For the chosen  $t_{\text{sb}}$  the initial energy in the wind bubble  $B_0$  does not influence the bubble energy at late times.

### 2.3 Numerical Method

All simulations were performed using the MHD implementation in GADGET-2 (Springel 2005), similar to that used in Dolag et al. (2005). Details of the MHD implementation can be found in Dolag & Stasyszyn (2008). The code is based on an entropy-conserving formulation of Smooth Particle Hydrodynamics (SPH) (Springel & Hernquist 2002). It was supplemented with a treatment of magnetic field using ideal MHD (see Dolag & Stasyszyn 2008). Besides following the induction equation for the magnetic field, we take magnetic back-reaction into account using a symmetric formulation of the Lorentz force based on the Maxwell tensor. The treatment of magnetic fields in SPH was improved by explicitly subtracting the part of the magnetic force which is proportional to the divergence of the magnetic field, as described in Børve et al. (2001). This helps to keep numerically induced divergence of the magnetic field at negligible values. It also helps to avoid instabilities of the MHD formulations in SPH, especially in regions where magnetic field pressure substantially exceeds the thermal pressure.

Note that in simulations without radiative cooling like ours the magnetic field pressure stays well below the thermal one, even within the cores of the most massive galaxy clusters. In very strong shocks however it can still happen that the magnetic field is compressed so substantially that magnetic forces dominate the thermal ones for brief periods of time. Such situations are handled more accurately with our new formulation, which includes several other, small improvements in the numerical treatment. For detailed investigations and information on the code and its performance see Dolag & Stasyszyn (2008).

## 3 SIMULATIONS

To identify galaxies in our simulations, we applied SUBFIND (Springel et al. 2001) which uses a friends-of-friends (FoF) algorithm to identify locally over-dense, self-bound particle groups associated with galaxies, even when they are inherited within a larger parent group. Originally, this algorithm was based on pure dark matter simulation, so we utilized a modified version to handle

Parameter	Value	Source
$R_0$	400 pc	(Klein et al. 1988)
$B_0$	50, 5, 0.5 $\mu\text{G}$	(Klein et al. 1988)
$B_G$	30, 3, 0.3 $\mu\text{G}$	(Chyzy & Beck 2004), (Soida et al. 2001)
$\dot{M}_*$	10 $M_\odot/\text{yr}$	(de Grijs 2001)
$t_{\text{sb}}$	150 Myr	(de Grijs 2001)
$M_{\text{ISM}}$	$< 3 \times 10^{12} M_\odot$	from simulation

**Table 1.** Summary of the parameters used for the wind model. Except for  $B_G$  all other parameters are based on observations of M82. The parameter set is scaled to the simulated galaxies by  $M_{\text{ISM}}$

the gas component as well (for more details see Dolag et al. 2008).

### 3.1 The Adopted Wind Model

To obtain the size and strength of the magnetic field in a starburst driven galactic outflow for each of the identified galaxies, we adapted the semi-analytical model by Bertone et al. (2006). This model assumes an adiabatic expansion of a spherical gas bubble with homogeneous energy density, fed continuously by the starburst-driven outflows. The initial bubble size (before the starburst) can then be characterized by a field strength  $B_0$  and a radius  $R_0$ . The bubble expansion is driven by the starburst in the galaxy, which is expelling gas at the rate  $\dot{M}_*$ , dragging the frozen-in magnetic field  $B_G$  into the ICM. The wind velocity is a function of the star formation rate, following Shu et al. (2005) we set the ISM constant  $K = 0.5$ , which determines the dependence of wind velocity and mass outflow rate on ISM properties (evaporation parameter and blast wave speed):

$$v_w = 320\sqrt{2} \cdot \left( \frac{\dot{M}_*}{M_\odot/\text{yr}} \right)^{0.145} \frac{\text{km}}{\text{s}}. \quad (1)$$

The galaxy thus injects magnetic energy into the wind at a rate

$$\dot{E}_{B_{\text{in}}} = \epsilon_{B_{\text{in}}} \frac{\dot{M}_w}{\bar{\rho}_{\text{in}}}, \quad (2)$$

where the injected mass rate is (Shu et al. 2005)

$$\dot{M}_w = 2.5 \left( \frac{\dot{M}_*}{M_\odot/\text{yr}} \right)^{0.71} \frac{M_\odot}{\text{yr}}, \quad (3)$$

and the average injected mass density  $\bar{\rho}_{\text{in}}$  follows from the injected mass blown through a spherical surface at the galactic radius, which is assumed to be a fraction of the virial radius  $R_g = 0.1 R_{200}$ :

$$\bar{\rho}_{\text{in}} = \frac{\dot{M}_w}{4\pi R_g^2 v_w}. \quad (4)$$

The injected magnetic field energy density  $\epsilon_{B_{\text{in}}}$  decreases adiabatically as  $B^2 \propto \rho^{\frac{4}{3}}$  (see App.A in Bertone et al. (2006)):

$$\epsilon_{B_{\text{in}}} = \frac{B_G^2}{8\pi} \left( \frac{\bar{\rho}_{\text{in}}}{\rho_{\text{ISM}}} \right)^{\frac{4}{3}}, \quad (5)$$

where  $\bar{\rho}_{\text{ISM}} = M_{\text{ISM}}/\frac{4}{3}R_G^3$  is the average ISM mass ( $M_{\text{ISM}}$ ) density inside a sphere of galactic radius. Finally, the predicted injected magnetic energy will be

$$\dot{E}_{B_{\text{in}}} = \frac{1}{2} B_G^2 R_G^2 v_w \left( \frac{\dot{M}_w R_G}{3v_w M_{\text{ISM}}} \right)^{\frac{4}{3}}. \quad (6)$$

Neglecting shear amplification the time evolution of the energy in the sphere is given by

$$\frac{d}{dt} E_B(t) = \dot{E}_{B_{\text{in}}}(t) - \frac{1}{3} \frac{\dot{V}_w(t)}{V_w(t)} E_B(t) \quad (7)$$

$$= \dot{E}_{B_{\text{in}}}(t) - \frac{1}{t} E_B(t). \quad (8)$$

Here local alignment between magnetic field and wind direction can not be assumed<sup>3</sup> because of turbulent instabilities and random motions in the gas. Still global structures might develop, because the magnetic field is dynamically unimportant and follows the preferred wind direction, parallel to the rotation axis of the halo. Figure 3 shows the evolution of the bubble energy as a function of the effective starburst time for several different values of the disc and halo parameters ( $B_G, B_0$ ) of the model. The model is based on a galaxy with ISM mass of  $M_{\text{ISM}} = 10 \times 10^{12} M_\odot$ . The initial bubble energy is diluted on reasonable starburst time scales, and therefore does not affect the final magnetic energy contained in the wind. The starburst time  $t_{\text{sb}}$  is therefore degenerate with  $B_G$  over a wide energy range. For more details on the wind model see Bertone et al. (2006).

Given the mass-cut on  $M_{\text{ISM}}$ , the resulting wind velocity is sufficient to reach every particle of a halo during the star-burst time scale assumed. Therefore we always seed the complete halo, by setting the magnetic field for every particle. Due to the friends-of-friends algorithm used to identify the structures, overlapping of halos is impossible and a minimum halo distance is defined by the linking length.

### 3.2 Applying the Wind Model

Contrary to Bertone et al. (2006), we cannot follow (and integrate) the evolution of the wind model over cosmic time based on semi-analytical modeling. Instead we are holding the numerical simulation at certain epochs and identify newly formed galaxies. We then integrate the wind model for every of these galaxies assuming a generic star-formation rate and a generic star-burst time. This effectively mimics the magnetic seeds obtained from such a galaxy at these epochs. The procedure is applied (in an approximate way) instantaneously. Given the mass-cut on  $M_{\text{ISM}}$ , the resulting wind velocity is so large that the wind can reach every particle within the virial radius of the halos during the assumed star-burst time scale. Hence, we are always seeding all particles within the virial radius, which by construction do not overlap. Continuing the magnetohydrodynamic simulation we follow the complete dynamics of the magnetized atmospheres, including their stripping and mixing in the denser environment (e.g. filaments or clusters atmospheres). The galactic virial radius selected for the seeding procedure is typically smaller than the radius of 100 kpc inferred for the wind driven bubbles in Bertone et al. (2006). The magnetised bubbles of the galaxy sized halos are stripped by ram pressure effects, which are already important in filaments (see (Dolag et al. 2006), (Saro et al. 2006), (Dolag et al. 2008)), as well as partially ejected by interactions with other galaxies. The stripped gas gets mixed with the cluster atmosphere, and large scale motions typically distribute this magnetized material across a much scale than the expanded bubble size predicted by the semi-analytical models.

The instantaneous seeding process is implemented in the simulations in the following way:

<sup>3</sup> This results in the factor 1/3 in the dilution term

- The simulation is stopped at the seeding redshift (usually  $z = 4.2$ ), and the newly formed galaxies (since the last seeding) are identified.

- The gas mass of the halos identified in the simulation is combined with the wind model to estimate the magnetic energy contained in the wind (see section 3.1).

- The magnetic moment of a dipole/quadrupole having the same magnetic energy is calculated. A smoothing length of 14 kpc is used as softening length in the integral (appendix A).

- The magnetic field vector of every gas particle in the corresponding halo is set to match the dipole/quadrupole. The field of every particle inside the softening length is set to a random orientation and the field strength at the softening length.

- The simulation is continued with the newly added magnetic field.

The parameters of the model can in principle be inferred from observations of individual galaxies. Table 1 shows some observational constraints on the parameters as obtained from one of the best observed, starbursting galaxies, M82. Note that in starbursting galaxies usually disc fields up to  $100 \mu\text{G}$  are observed (R.Beck, priv.com.). This is the case on scales smaller than the resolution achieved by our simulations (14 kpc). We rather follow the conservative approach in Bertone et al. (2006) using a field of several tens of  $\mu\text{G}$ .

M82's observed mass of  $6 \times 10^9 M_\odot$  (Sofue 1998) is smaller than the average mass of the seeded halos (table 2). To take this into account, we assume that the mass of the ISM  $M_{\text{ISM}}$  in the model is equal to that of the halo mass in the simulation, and not from M82. There is further mass dependence in the mass outflow rate  $\dot{M}_*$ . Therefore the value inferred from M82 might be underestimated and the obtained wind energy represents a lower limit for large halos.

As the values quoted are still quite uncertain, we performed simulations where we varied the value for the halo and disc magnetic field ( $B_0, B_G$ ) within a wide range.

The magnetic field structure within galactic outflows and the properties of the resulting wind driven bubble are largely unconstrained as well. In M82, Reuter et al. (1994) observe a symmetric poloidal magnetic field structure in the core, while in edge-on galaxies combinations of symmetric (S0) and antisymmetric (A0) field structures are observed (R.Beck, priv.com.). A0 and S0 dynamo modes can be approximated by a softened dipole and quadrupole field structure, respectively. We therefore describe the structure of the magnetic seed field as a (softened) dipole field, which we normalized so that the field energy corresponds to the energy in the magnetic bubble inferred from our semi-analytical model. The orientation of the dipole is chosen to align with the spin of the underlying dark matter halo. To verify the dependence of our results on the detailed structure of the seed fields we also performed a run where we used a quadrupole instead of a dipole structure for the magnetic seed field.

Including the reference run (*Control Run*) which follows the evolution of a cosmological seed field, we performed six different simulations to explore the parameter space. In all runs the starburst time  $t_{\text{sb}}$  is kept fixed at 150 Myr. We performed three simulations for different values of the magnetic fields (halo  $B_0$  and disc  $B_G$ ) which all have a dipole like structure. Starting from the M82 like value of  $50 \mu\text{G}$  (*Dipole*), we also performed a run with one tenth of the value (*0.1 Dipole*) and one hundredth (*0.01 Dipole*). We used the *Dipole* parameter set from above to perform a run with

Snapshot	Redshift	$N_{\text{halos}}$	$\langle M_{\text{halos}} \rangle [M_\odot]$
8	4.1	24731	$1.2 \times 10^{11}$
10	3.2	10483	$6.9 \times 10^{10}$
12	2.5	12467	$6.7 \times 10^{10}$
14	1.9	11326	$6.6 \times 10^{10}$
16	1.4	9838	$6.6 \times 10^{10}$

**Table 2.** Halo statistics of the multiple seed run. The rows give the output number, the corresponding redshift, the number of new haloes identified since last seeding and the mean mass of these haloes, respectively.

a quadrupole structure (*Quadrupole*). We further repeated the *0.1 Dipole* run and performed four additional seeding episodes (*Multi Seed*) to all newly formed haloes as summarized in table 2. From the results (e.g. compare left and right panel in the middle row of figure 5) its clear that after the first seeding, many new haloes are still seeded, but they are typically smaller in mass (see last column in table 2) and preferentially located outside the proto-cluster region.

## 4 GENERAL RESULTS

Figure 4 shows the results from the two different seeding strategies compared in this work. The right column shows the case of primordial magnetic seed field (*Control Run*) and the left column a run which used the seed fields of galactic outflows (*Dipole*). Shown is the magnetic field amplitude projected through the box. The top row shows the field at the first seeding of the galactic outflows while the lower row shows the final magnetic field at redshift zero. One can clearly see the differences between the two models at early times: the low-level primordial magnetic field fills the whole volume, whereas the magnetic field from the galactic outflows is concentrated on the galaxy population. At low redshift the magnetic field in galaxy clusters appears comparable in both models. This reflects the fact that inside the galaxy clusters the magnetic field is strongly processed by compression, shear flows and turbulence. Therefore, the final magnetic field is shaped by such processes rather than by the initial conditions, in agreement with previous findings (Dolag et al. 1999, 2002) and analytical modeling of saturated dynamos in clusters (Subramanian et al. 2006; EnBlin & Vogt 2006). However, the magnetic field in filaments looks quite different. In the model with galactic outflows the magnetic field in the collapsed objects along the filaments is higher than for a primordial seed field; the magnetic field inside the diffuse component of the filaments is much more prominent in the case of cosmological seed fields,

because the density in the filaments is too low to strip the hot and magnetized atmosphere of the galactic halos completely. Note that our models do not include a kinematic component which could lead to an evaporation of the haloes around galaxies. This and especially the effect of AGN-driven outflows could change the picture, as the outflows could fill volumes of Mpc size in these low density environments (see Kronberg (2006), and references therein). We also note that in principle small galactic halos (down to masses of  $10^8 M_\odot$ ) – which are not resolved in the simulation – could contribute to the magnetization of the low density environment. However, observations suggest that the star-formation rate of such galaxies would be quite small (far below the value of  $10 M_\odot/\text{yr}$  Daddi et al. (2007) adopted in this work for resolved galaxies). Wence, we do expect them to contribute significantly.

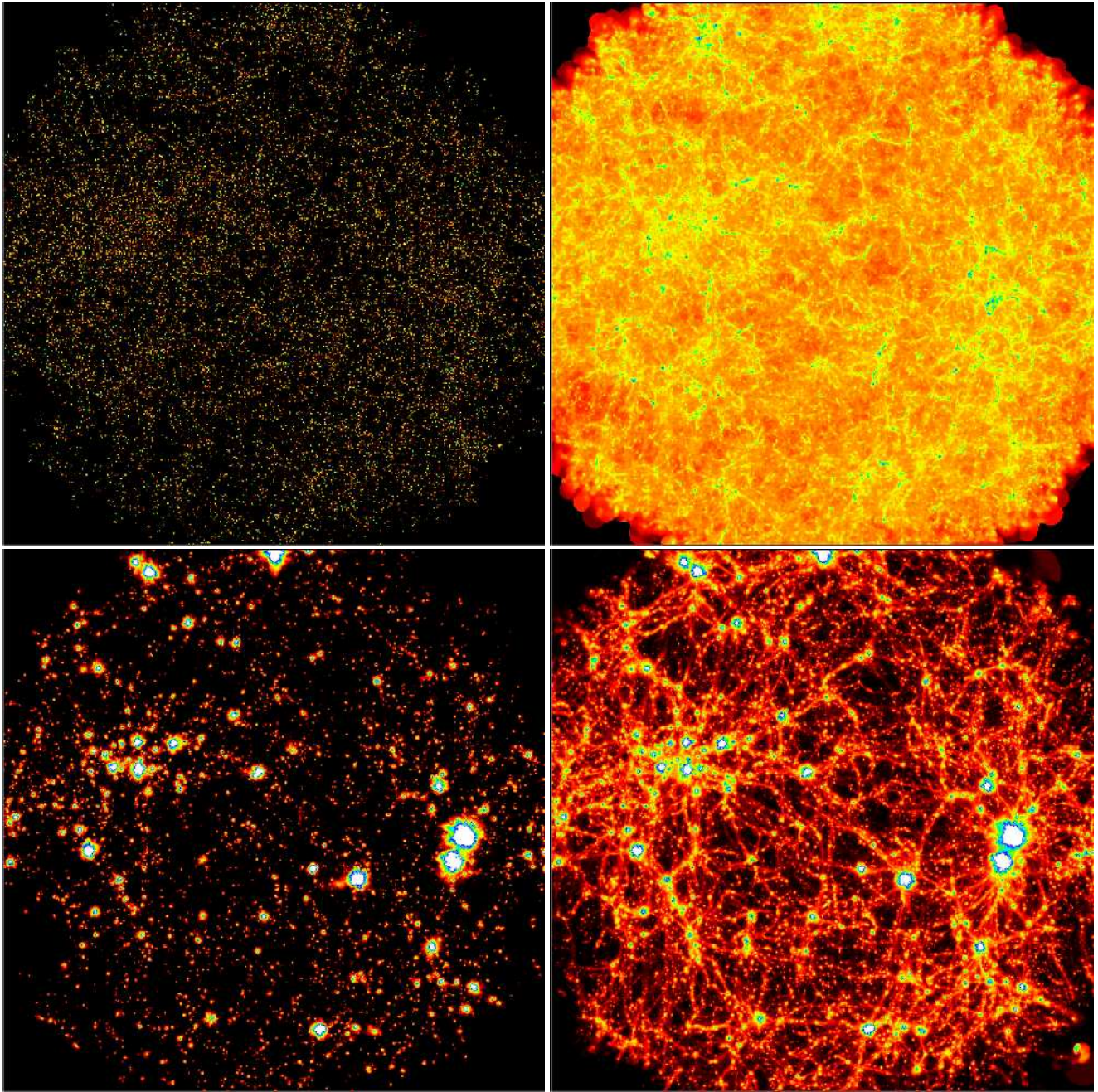


**Figure 4.** Visualisation of the magnetic field strength in the simulation box at redshifts  $z = 4.1$  and  $z = 0$ . Every image shows a region of a linear size of  $204 \text{ Mpc}/(1+z)$  and was made using the same color bar. The upper left panel shows the magnetic field due to instantaneous seeding with a dipole M82-like structure at this redshift with maximum field strengths of  $\approx 5 \text{ nG}$ . The upper right shows a simulation with homogenous cosmological magnetic seed field (Dolag et al. 2005). Here, the field strength more continuously traces the underlying structures of the matter distribution and reaches values of up to  $\approx 10 \text{ nG}$  in the highest density regions. The lower two panels show both simulations (left *Dipole*, right *Control Run*) evolved to  $z = 0$ .

Figure 5 shows the magnetic field amplitude projected through the box for all different runs at redshift zero. When the halo magnetic field in the wind model is reduced, the field within the individual galaxies is strongly reduced. Therefore the magnetic fields within the filaments become less prominent (*Dipole*, *0.1 Dipole* and *0.01 Dipole* panels). However, the magnetic field within the collapsed structures of galaxy clusters only slightly changes, indicating that the amplification within the cluster centers is strongly influenced by saturation effects, well in agreement with previous findings (Dolag et al. 2005). The situation changes for the multi

seed run (*Multi Seed*). Although again the magnetic field in the clusters is not affected, a clear change is visible in the filaments, where many more seed fields from galaxies appear. This is because galaxies are formed earlier in high density environments like proto-cluster regions than in low density environments, like filaments. Subsequent seeding of newly formed haloes therefore preferentially happens in low density environments like filaments.

A more quantitative way of displaying the differences of our models is to show the volume weighted cumulative filling factors obtained within the whole box. In figure 6 the rising (falling) curve

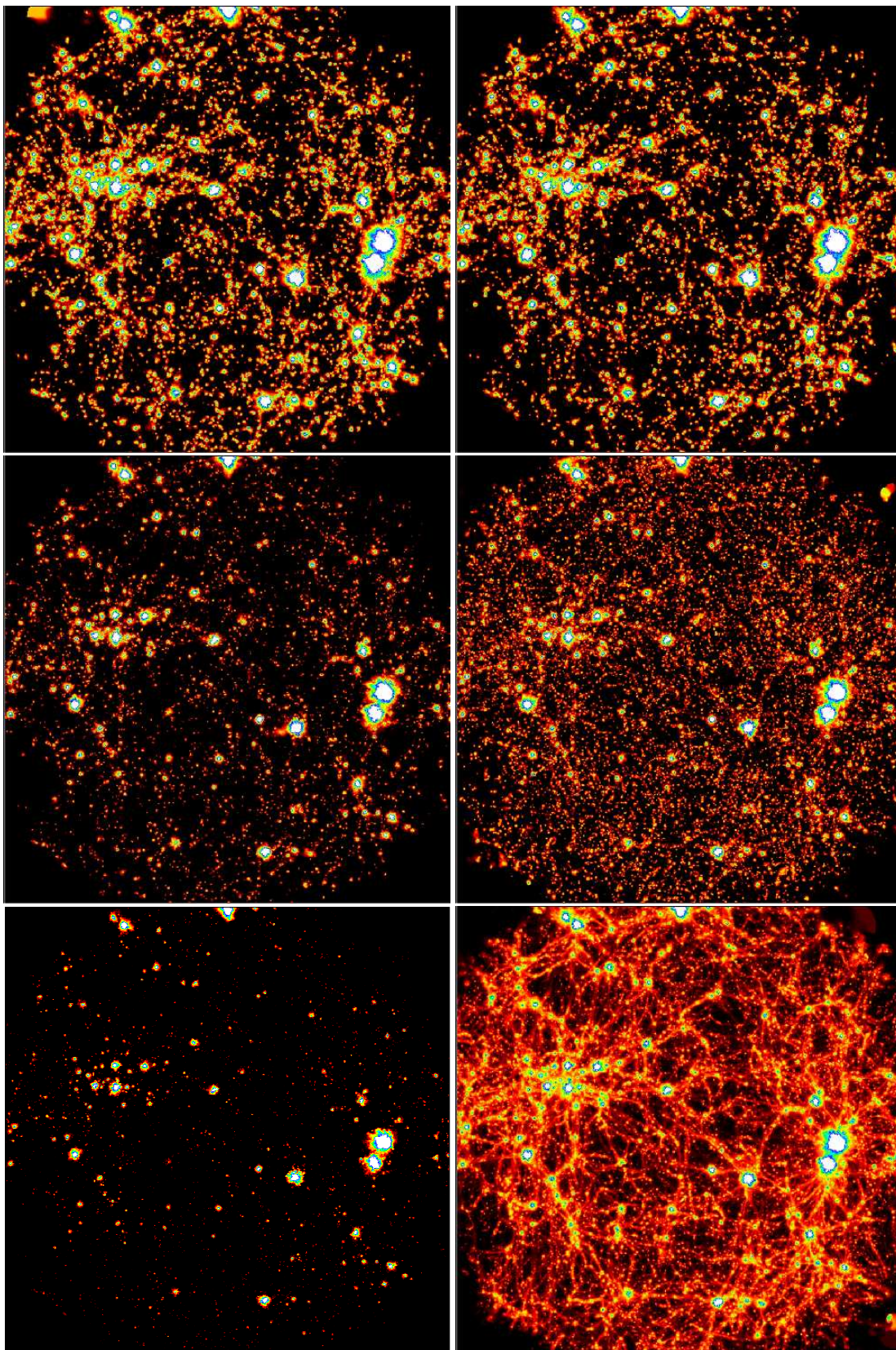


**Figure 5.** Visualization of the magnetic field strength in the simulation box at redshift  $z = 0$ . Every image shows a region of  $204 \text{ Mpc}/(1+z)$ , using the same arbitrary color bar. Shown are the results of the *Dipole* (top left), *0.1 Dipole* (middle left), *0.01 Dipole* (bottom left), *Quadrupole* (top right), *Multi Seed* (middle right), and the *Control* simulation (bottom right), respectively.

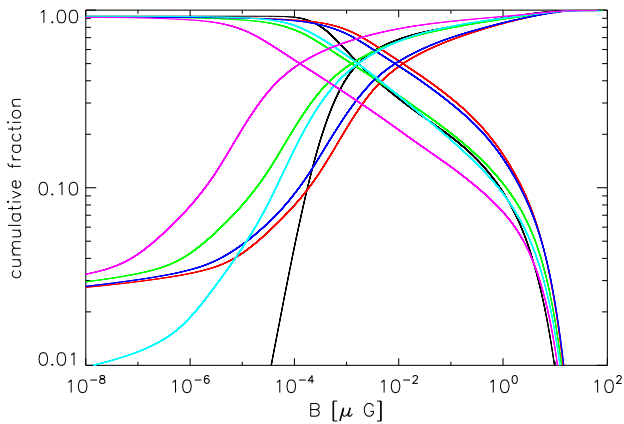


**Figure 6.** Volume-weighted cumulative filling factor of the magnetic field in the cosmological box. The filling factor is plotted above and below a threshold as a function of the threshold (the rising and falling curves). The black lines show the cosmological seed field from Dolag et al. (2005). Also shown are the wind-induced seeding from the *Dipole* (red) and *Quadrupole* (blue) and the curves from the simulations with decreased field strength (green curve: *0.1 Dipole*; magenta curve: *0.01 Dipole*). The results from the simulations with the *Multi Seeds* are given by the light blue curve.

indicates the relative filling of the box by a magnetic field weaker (stronger) than a certain value, for all simulations at redshift  $z = 0$ . In the very high field regime ( $\mu\text{G}$  and above) all simulations behave similar to each other, again indicating that amplification within galaxy clusters is strongly influenced by saturation effects. In the intermediate regime (most visible in the rising curves), the simulations split in three groups, distinguished by the chosen value for the disc magnetic field, which controls the amount of magnetic field within the galactic outflow. In this regime, magnetic field amplification reflects the underlying velocity field structure. The simulation, which evolves a cosmological seed field (*Control Run*), corresponds (by chance) to a medium value of the galactic fields (*0.1 Dipole*). At low magnetic field (best visible in the rising curves), the filling factor is dominated by the properties of the seed field. Therefore, all models are clearly distinguishable. This region corresponds to the low density regions, including the diffuse matter in filaments. For lowest fields, the four single seeded simulations converge to a non zero value, representing the un-magnetized volume left in the box. The multi seeded simulation shows a lower fraction of unmagnetized volume, which is expected from the seeding strategy. In the simulation using a cosmological seed field, no volume is filled with a field smaller than this seed field (adiabatically diluted with the local density).

This shows that for galaxy clusters the single seed simplification in our approach is not crucial. On the other hand, low density regions like filaments provide a natural testbed for the origin of cosmological magnetic fields and also are very sensitive to the approximations and simplifications made.

This is expected from previous findings. In simulations where a cosmological magnetic field is evolved, the field amplification is linear in low density regions undergoing mainly adiabatic compression or dilution, whereas the orientation is typically aligned with the filament (Dolag et al. (2005); Brügggen et al. (2005)). Therefore, such regions are only mildly influencing the magnetic field configuration imposed by the seeding mechanism.

## 5 CLUSTER BASED ANALYSIS

The amplification of magnetic fields in galaxy clusters is driven by adiabatic compression, and merger events, which induce shear flows and subsequent turbulent flows. All these processes depend on the cluster environment and therefore may depend on cluster mass. Observationally there is yet not enough data available to track how the magnetic field varies within clusters as function of radius or how the mean field within the cluster varies with cluster mass (or equivalent, with the mean cluster temperature). Cassano et al. (2007) concluded from the properties of observed, diffuse radio emission (so-called radio halos) that the mean magnetic field within the radio emitting region appeared independent of cluster mass.

But the volume of the radio-emitting region is found to increase with cluster mass.

Therefore, even if the central magnetic field does increase with cluster mass, a constant mean magnetic field could still be inferred, if the shape of the radial field profile decreases properly. Furthermore, although indications for a radial dependence of the magnetic field can be inferred from clusters where rotation measures of several radio galaxies are available (Dolag et al. 2001; Murgia et al. 2004; Govoni 2006), there exists still a large degeneracy between the parameters describing the magnetic field in clusters (Bonafede et al. 2008; Guidetti et al. 2008). Hence, it is quite important to compare observed scalings with predictions from simulations. Especially the dependence of scaling relations on the adopted model for the origin of the magnetic seed fields has to be studied in more detail. To this end, various simulations performed in the past gave quite different results.

Models based on shock induced field generation predict magnetic field strengths with a very weak dependence on the distance to the cluster center and also predict a scaling of the mean magnetic field  $B \propto \sqrt{T}$  (Miniati et al. 2001).

In contrast, previous SPH simulations following a primordial magnetic seed field predict a steep radial dependence for the mean magnetic field, mainly following the decline of the density (Dolag et al. 2001, 2005). Such steep profiles were confirmed with AMR simulations (Brügggen et al. 2005; Dubois & Teyssier 2008). SPH simulations also predict a very steep correlation of the mean magnetic field with the cluster temperature, e.g.  $B \propto T^2$  (Dolag et al. 1999).

### 5.1 Radial profiles

In figure 7 we plot angularly averaged radial profiles of density (left column) and mass-weighted temperature (right column). The individual lines are taken from the 16 most massive clusters within the simulation. They are scaled to the virial radius of the individual clusters and are normalized to the same mean value within  $0.1R_{\text{vir}}$ . The upper row shows the results from the control run following a primordial magnetic seed field (Dolag et al. 2005), the lower row shows results from the dipole run with the largest value for the galactic halo field. Although individual haloes show small variations because of the slight changes magnetic fields introduce in the systems dynamics (by adding small perturbations of the force field at high redshift), there is no significant dynamical influence of the magnetic field. This is in good agreement with the relatively small values of the magnetic fields ( $< 10\mu\text{G}$ ) within the simulated galaxy clusters, and also with previous results.

Figure 8 shows the RMS magnetic field profiles for the 16 most massive clusters for all our simulations. As before, they are

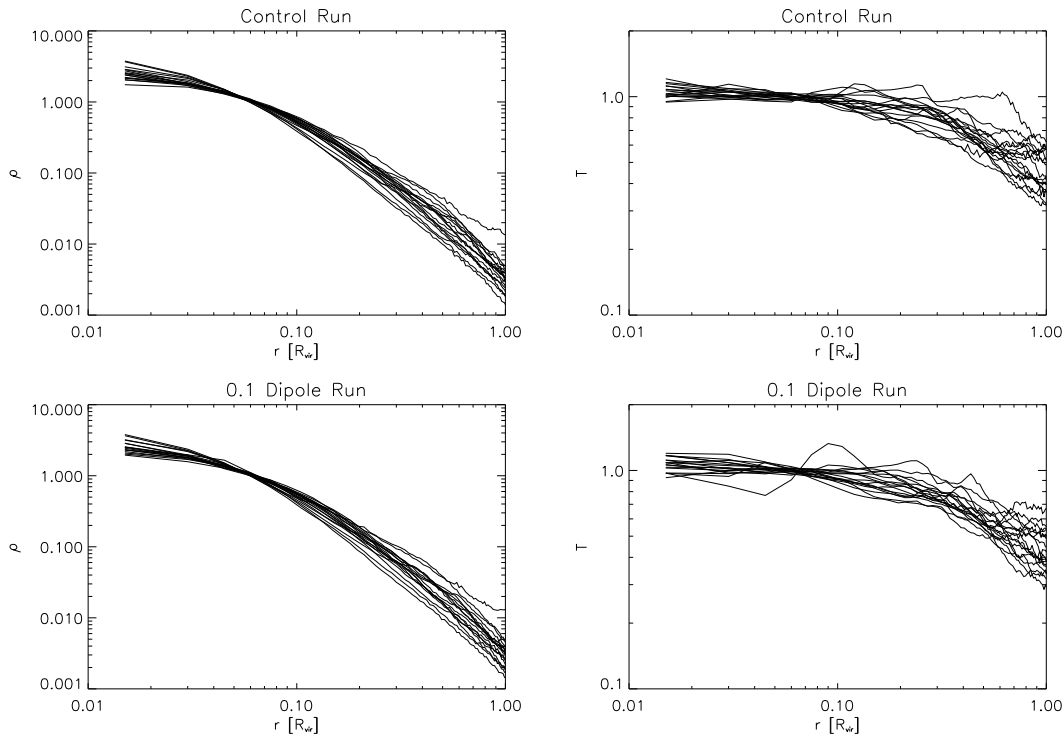


**Figure 7.** Density (left column) and mass weighted temperature (right column) profiles for the 16 most massive clusters in the simulations. Here, only the *Control Run* and the *Dipole Run* are shown, demonstrating the absence of a significant dynamic influence of the magnetic field in the models.

scaled to the virial radius of the individual clusters and are normalized to the same mean value within  $0.1R_{\text{vir}}$ . In good agreement with previous findings, the magnetic field profiles generally follow a very similar decline as the density, but with somewhat more scatter. However, the scatter of the individual magnetic field profiles seems to depend on the overall strength of the magnetic field. The simulations with higher magnetic seed fields (e.g. the *Dipole* and *Quadrupole* runs) show significantly less scatter. This is a clear indication that in these simulations saturation effects dominate the amplification of the magnetic field in outer parts. Therefore, the total field amplification is less dependent on the system's dynamics and so the differences in the scaled profiles are reduced. There is also some indication that the scatter in the profiles is slightly increased for the *multiple seed* run, indicating that there could be still some influence of the late forming galaxies on the outer parts of the magnetic profiles. In general, aside from the scatter in the profiles the exact details of the origin of the magnetic seed fields do not strongly influence the predicted shape of the radial profiles. Therefore, the shape of the magnetic profiles is a robust prediction of the simulations, driven mainly by the dynamics imprinted from the structure formation process.

## 5.2 Average field strength

Figure 9 shows the mean magnetic field within one tenth of the virial radius as a function of mean, mass-weighted temperature for the 16 most massive clusters from our simulations. There is a strong trend of the magnetic field with temperature (e.g. mass). At low temperatures (e.g. low masses) a large scatter is present, not only for models with different seed fields, but also for clusters with similar temperature. Simulations of low mass/temperature systems also show a quite steep relation, indicating that for small systems, the

dynamical state is very important. Here, the magnetic field amplification is still in a regime, where individual merger events strongly contribute to the amplification of the magnetic fields. At intermediate and high temperatures the scatter reduces and the trend becomes very regular. For strong magnetic field models the mean field flattens horizontally as a function of temperature, which indicates a saturation of the magnetic field amplification. This can be seen well when comparing runs with varying dipole strength (left column of figure 9). Again, there is no significant dependence on the original magnetic field structure assumed within the galactic outflows as evident from comparing the *0.1 Dipole* with the *Quadrupole* simulation. *Multi Seed* simulations only affect low mass systems.

The normalisation of the average magnetic field strength might be sensitive to the resolution of the simulation, as well as to the exact details of saturation of the amplification mechanism. This includes the final amplitude of the mean magnetic fields as well as the temperature (mass) scale at which clusters magnetic fields reach the saturation regime. The central magnetic fields (several  $\mu\text{G}$ ) found in our simulated clusters are in good agreement with observations (e.g. see values of Guidetti et al. 2008; Govoni et al. 2006; Murgia et al. 2004; Bonafede et al. 2008).

## 5.3 Synthetic rotation measurement profiles

To compare the simulated magnetic field from different seeds with observations, we repeat the comparison with observational data as in (Dolag et al. 2002, 2005). Figure 10 shows a combination of three observational samples, measuring the Faraday rotation of point like sources in or behind Abell clusters as function of their distance to the center of the clusters (Kim et al. 1991; Clarke et al. 2001; Johnston-Hollitt & Ekers 2004). The black line shows the result obtained for the median of the absolute values when radially

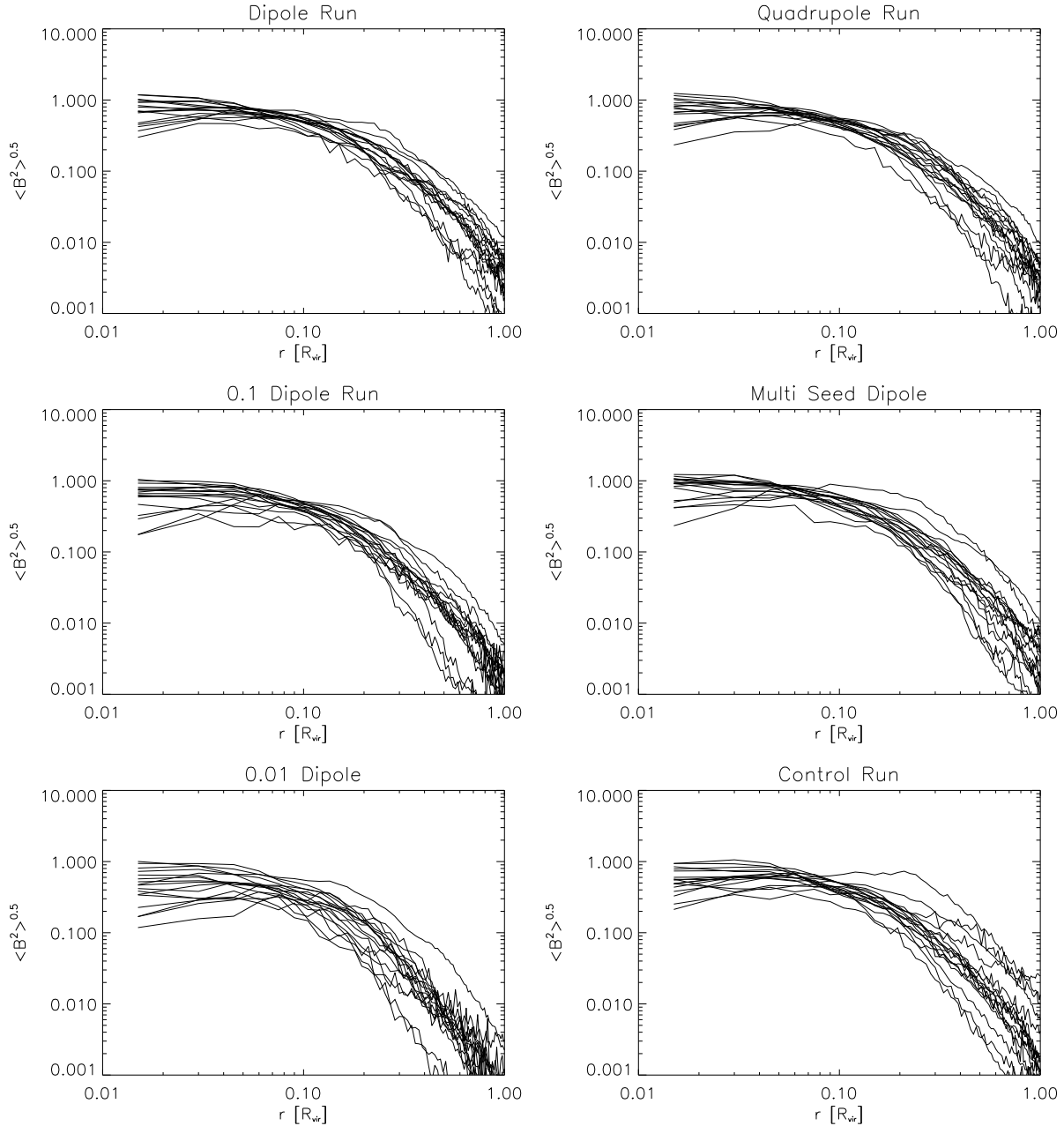


**Figure 8.** Radial profiles of the RMS magnetic field strength for the 16 most massive clusters. The profiles are scaled to  $R_{\text{vir}}$  and normalized to the same mean value within  $0.1 \times R_{\text{vir}}$ . Shown are the results of the *Control* simulation (bottom right), *Dipole* (top left), *0.1 Dipole* (middleleft), *0.01 Dipole* (bottom left), *Quadrupole* (top right) and *Multi Seed* (middle right), respectively.

binning using bins of 15 data points each. All three individual samples are statistically compatible with each other and we combine all of them to allow a finer binning of the data. To calculate error bars we used the RMS of the median obtained by bootstrapping the samples of each bin 1000 times. We over plotted the values inferred from three elongated sources (triangles) observed in the single galaxy cluster A119 (Feretti et al. 1999) and one elongated source within the Coma cluster (diamonds) (Feretti et al. 1995). As discussed in previous work (Dolag et al. 2005), due to the construction of these observational samples, the underlying selection function for the contributing galaxy clusters is ill-defined. This is especially important, as the signal depends on the mass of the un-

derlying galaxy clusters, both due to the larger line of sight contribution from massive systems as well as the predicted dependence of the magnetic field strength on the cluster mass. One therefore expects the median profile to depend on the mass function of the selected clusters. However, as the cluster sample is composed of Abell clusters, it is reasonable to assume that it mainly consists of comparatively massive galaxy clusters. The additional data points inferred from the two massive systems A119 and Coma (black symbols) follow the curve from the combined sample (black line) reasonable well, indicating that the observed sample indeed compares well to the predictions for more massive systems.

From the simulations we calculated synthetic Faraday rotation

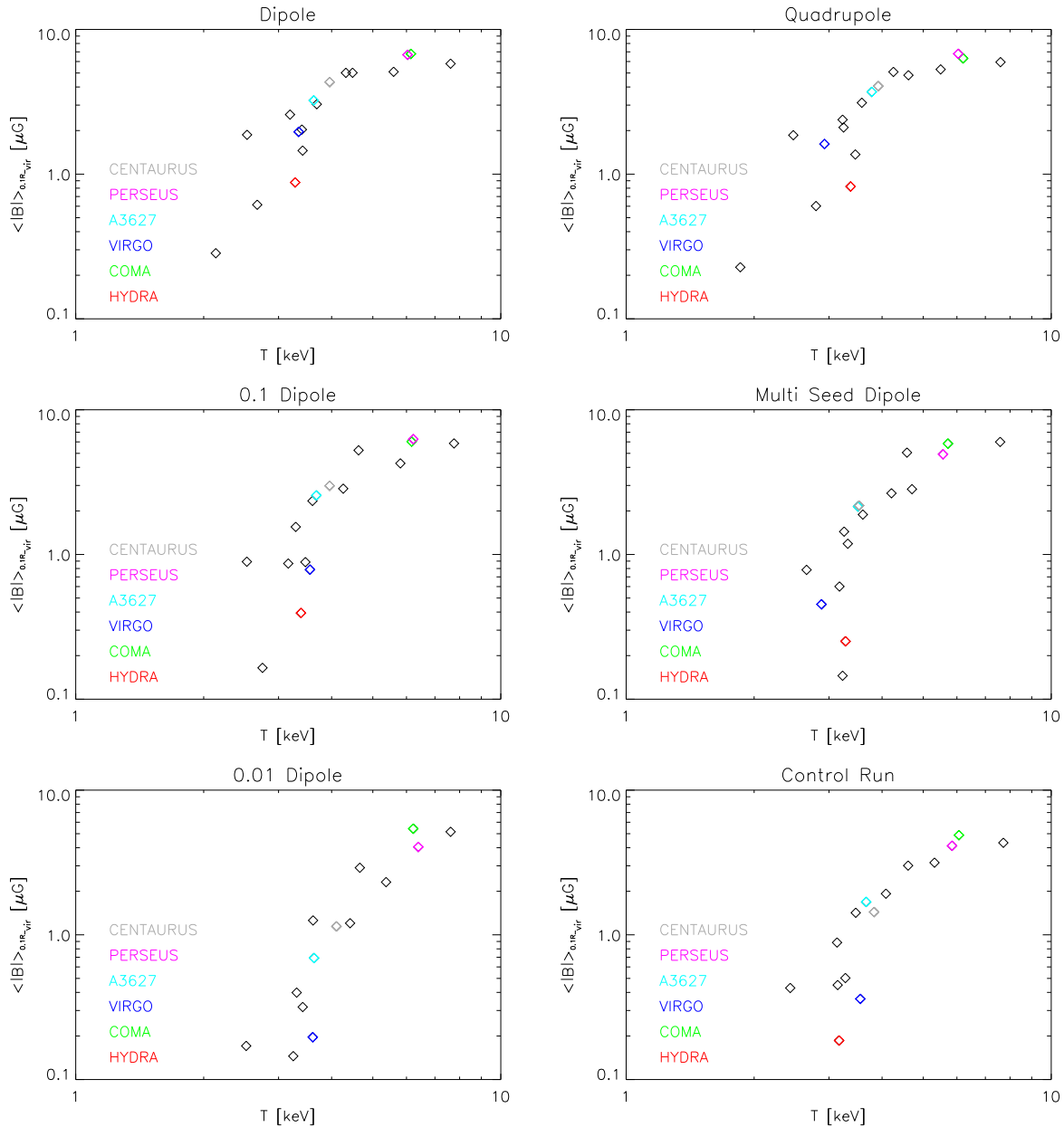


**Figure 9.** Same arrangement as figure 8 showing the mean magnetic field strength inside one tenth of the virial radius as function of the mean, mass-weighted temperature within the same radius. Clusters that have an observed counterpart are marked with different colors.

maps for the 16 most massive clusters. Binning the individual maps in radial bins we computed the median of the absolute value of the Faraday rotation combining the same radial bins from all clusters. This procedure was repeated for two subsets of the clusters, where we restricted the sample to clusters with masses above  $3 \times 10^{14} M_{\odot}$  and  $5 \times 10^{14} M_{\odot}$  respectively. The results are shown as three colored lines in figure 10. In general, the shape of the resulting radial profiles compares to observations quite well; there is in particular no noticeable difference between the *Control* run, which follows the evolution of a primordial magnetic field and the *Dipole 0.1* run. The *Dipole 0.1* fits also best regarding the different strength for the galactic halo field. In agreement with results presented before, there is no visible difference between the quadrupole and the dipole configurations for the magnetic field in the galactic winds. There are

also only very mild effects visible in the outer parts of the Faraday rotation profiles for our run with the multiple seeding episode.

Finally, we calculated the projected structure function from some of the synthetic Faraday rotation maps. This was done following Murgia et al. (2004), who calculated this for observed Faraday rotation maps:

$$S^{(1)}(dx, dy) = \langle |RM(x, y) - RM(x + dx, y + dy)| \rangle, \quad (9)$$

with  $dx$  and  $dy$  being the offsets from a pixel at position  $(x, y)$ . The resulting matrix is then averaged in radial bins to finally obtain the structure function. In figure 11 we show the structure functions obtained from three of our clusters normalized at the largest scales. For the different models of the magnetic seed field the structure functions only reveals some small differences in the Faraday

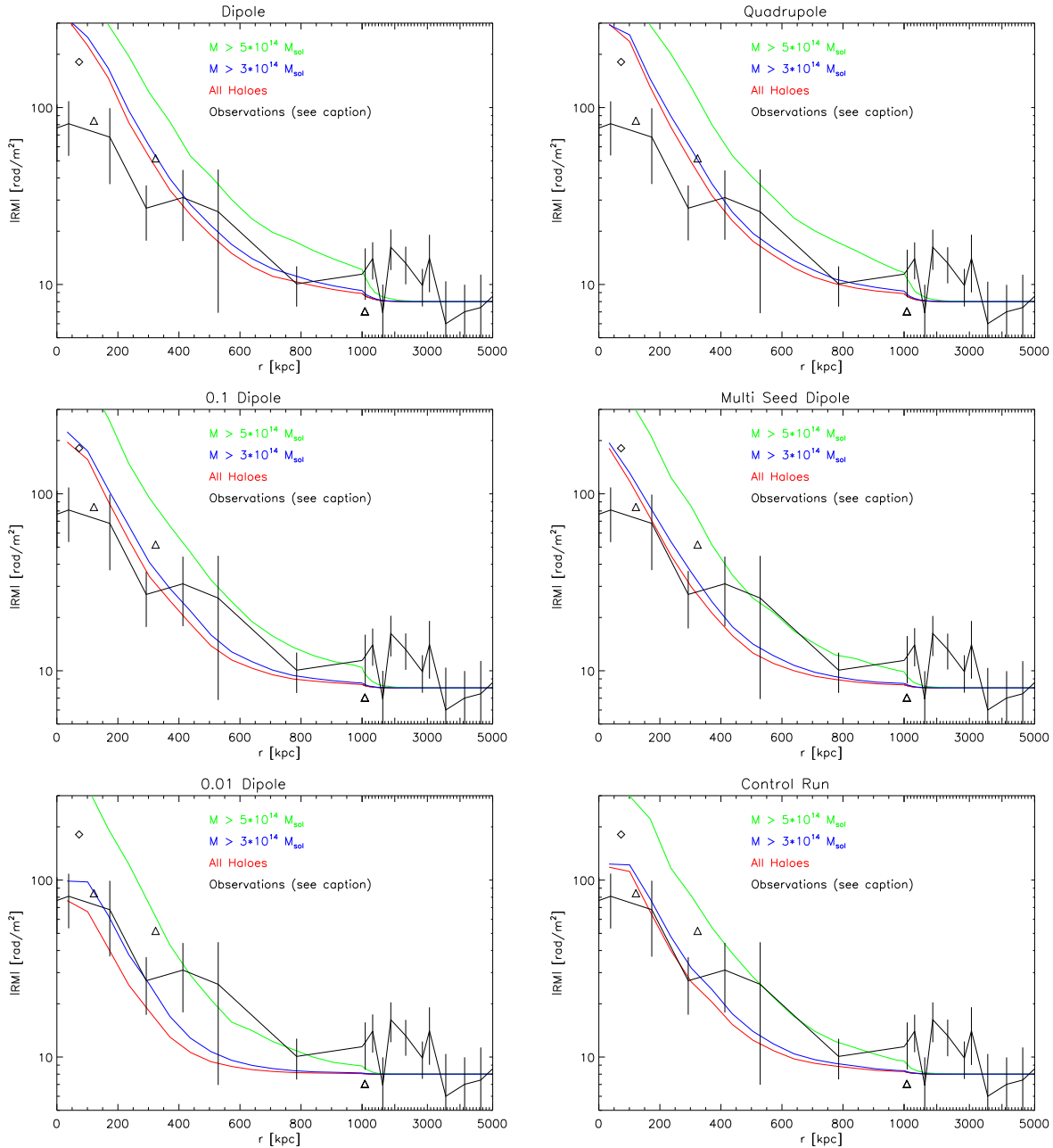


**Figure 10.** Same arrangement as figure 8 but showing the radial profiles of Faraday rotation. We binned the absolute value of the observed Faraday rotation as function of distance to the centres of the clusters and plotted the median forcing the radial intervals to contain always 15 data points. The data are obtained from combining three samples based on Abell clusters (Kim et al. 1991; Clarke et al. 2001; Johnston-Hollitt & Ekers 2004). The error bars are obtained by bootstrapping the data points within each bin. We also included in the plot the values inferred from three elongated sources (triangles) observed in the single galaxy cluster A119 (Feretti et al. 1999) and one elongated source within the Coma cluster (diamond) (Feretti et al. 1995). For the simulations we build the median of the Faraday rotation for the 16 most massive clusters (red line) and subsets restricting their mass to be larger than  $3 \times 10^{14} M_{\odot}$  and  $5 \times 10^{14} M_{\odot}$ , blue and green line respectively.

rotation of the first cluster. In general, there are no significant indications of the seed magnetic field in the final Faraday rotation structure, especially given that the effective resolution limit of the simulation is about 15 – 20 kpc in the central parts of the clusters.

## 6 CONCLUSIONS

In this work we performed cosmological, magnetohydrodynamic simulations following the evolution of magnetic fields on large scale structures and in galaxy clusters. Coupling a semi-analytic model for magnetized galactic winds as suggested by Bertone et al. (2006) with our cosmological simulation we explored the possibility that the magnetic fields in galaxy clusters originate from galactic outflows during star-burst phases, further processed by struc-

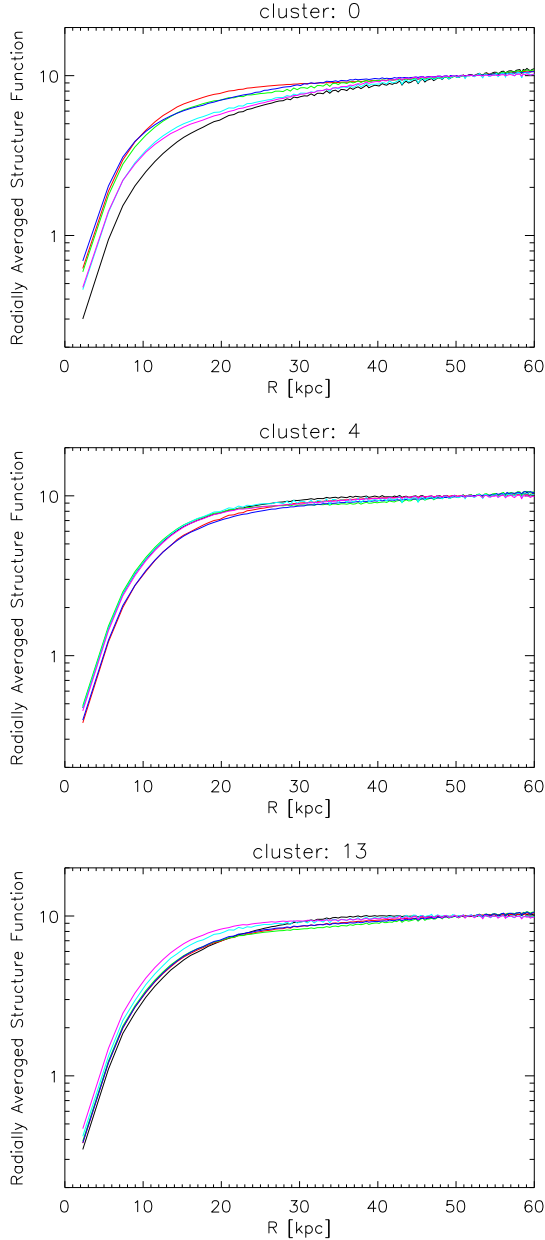


**Figure 11.** Shown is the structure function (for details see text) calculated from synthetic Faraday rotation maps obtained from different clusters displayed in the individual panels. The different lines correspond to different magnetic seed fields.

ture formation. We compared our results with the ones obtained by following a primordial magnetic seed field (Dolag et al. 2005). Performing several simulations, we explored the effect of various parameters of the adapted semi-analytic model relevant for the strength of the magnetic seed field from the galactic outflows. We also explored the effect of the magnetic field configuration assumed for the galactic outflows and of the seeding strategy. Our general findings are:

- The typical magnetic field strengths of several  $\mu\text{G}$  in galaxy clusters as obtained from observations of Faraday rotation are well reproduced for a wide range of parameters of the galactic outflow model.

- The general shape of the predicted Faraday rotation profile within clusters compares well with the sparse observational data available. Models that assume a field strength of  $5\mu\text{G}$  within the galactic halo reproduce the observed Faraday rotation profiles better than models with a ten times stronger or a ten times weaker halo magnetic field.

- The properties of the final magnetic field in galaxy clusters do not depend on the exact field configuration within the magnetic outflows. This confirms previous studies that the structure of the magnetic field in galaxy clusters is primarily driven by the velocity field induced by the structure formation process.

- In massive galaxy clusters, the magnetic field amplification saturates around values of several  $\mu\text{G}$ . The mass (or temperature) scale on which this happens depends on the strength of the magnetic seed field, and probably also on the resolution of the simulation.

- In systems where saturation effects start to play a significant role, we observe only a small scatter in the magnetic scaling relations, and in the shape of the radial, magnetic profiles.

- In clusters where saturation effects are negligible the strength and configuration of the magnetic field strongly depends on the dynamic state. Therefore, we observe a large scatter in the magnetic scaling relations and in the shape of the radial, magnetic profiles.

- Within galaxy clusters, the structures predicted from synthetic Faraday rotation maps do not depend significantly on the magnetic seed field, and agree well with observed ones.

- In low density environments imprints of the magnetic seed fields are still present and can be observed, in principle. In these environments the galactic outflows forming at later epochs contribute significantly to the magnetic field configuration.

In summary, we confirm that galactic outflows and the subsequent action of structure formation can explain the properties of the magnetic fields observed in massive galaxy clusters. Their strength and shape is attributable to the velocity field induced by structure formation. We find that there are no measurable imprints of the magnetic seed fields left in the synthetic Faraday rotation maps of our simulated clusters. However, low density environments, like filaments, still contain significant information on the magnetic seed fields. Therefore, they may be used to discriminate proposed scenarios once information on magnetic fields within these regions becomes available with the next generation of radio instruments.

## ACKNOWLEDGMENTS

We want to thank Caroline D’Angelo for carefully reading and improving the manuscript.

## APPENDIX A: CONVERSION FORMULAE

### A1 Dipole Energy

$$E_B = \frac{1}{8\pi} \int \vec{B}^2 dV \quad (\text{A1})$$

$$\vec{B} = \frac{1}{4\pi} \frac{3\vec{n}(\vec{n} \cdot \vec{m}) - \vec{m}}{|\vec{r}|^3} \quad (\text{A2})$$

To calculate the magnetic moment  $\vec{m}$  of a dipole of magnetic energy  $E_B$ , one assumes, that  $\vec{m} \parallel \vec{e}_z$ , as the moment can be aligned into any other direction by a simple rotation of the coordinate system. The unit vector  $\vec{n}$  then becomes  $z/|z|$ .

Since the field  $\vec{B}$  diverges for  $r \rightarrow 0$  we use a softening length of  $\epsilon = 14$ , which corresponds to the SPH smoothing length. The outer boundary  $R_{\max}$  takes the finite size of the halo into account. Setting  $\mu_0 = 1$  it follows:

$$\begin{aligned} E_B &= \frac{1}{8\pi} \int \frac{1}{(4\pi)^2} \frac{(3\vec{n}(\vec{n} \cdot \vec{m}) - \vec{m})^2}{(|\vec{r}|^3 + \epsilon^3)^2} dV \\ &= \frac{1}{120\pi^3} \int \frac{dV}{(|\vec{r}|^3 + \epsilon^3)^2} \cdot \left( 3 \left( \frac{z}{|\vec{r}|} m_z \right)^2 + m_z^2 \right) \\ &= \frac{m_z^2}{4(4\pi)^2} \cdot \int_0^{R_{\max}} \int_0^\pi \frac{3r^2}{(r^3 + \epsilon^3)^2} \cdot \sin \phi \cos^2 \phi \, dr \, d\phi + \\ &\quad \frac{m_z^2}{4(4\pi)^2} \cdot \int_0^{R_{\max}} \int_0^\pi \frac{r^2}{(r^3 + \epsilon^3)^2} \cdot \sin \phi \, dr \, d\phi, \end{aligned}$$

where we used spherical coordinates. It follows

$$m_z = \sqrt{48\pi^2 E_B \cdot \left( \frac{1}{\epsilon^3} - \frac{1}{R_{\max}^3 + \epsilon^3} \right)^{-1}}. \quad (\text{A3})$$

## A2 Quadrupole Energy

We constitute the quadrupole as a superposition of 2 dipoles at a distance  $d$ , with dipole moments  $\vec{m}_1 = m_z \vec{s}$  and  $\vec{m}_2 = m_z (-\vec{s})$ , “pointing” into opposite directions. Introducing a softening length  $\epsilon$ , the field is given by

$$\vec{B} = \vec{B}_+^{\text{DIP}} + \vec{B}_-^{\text{DIP}}$$

As the field energy does not depend on the direction of the dipole

$$E_B = \frac{2}{8\pi} \int \vec{B}^2 dV + \frac{2}{8\pi} \int \vec{B}_+ \vec{B}_- dV.$$

We define

$$\begin{aligned} \vec{r}_\pm &= \vec{r} \mp \frac{d}{2} \vec{s}, \\ r_\pm &= |\vec{r}_\pm|, \\ \vec{n}_\pm &= \frac{\vec{r}_\pm}{r_\pm}, \\ n_\pm^z &= \vec{n}_\pm \cdot \vec{e}_z, \\ \vec{m}_\pm &= \pm m_z \vec{s}, \end{aligned}$$

and the field energy becomes

$$E_B = \frac{2m_z^2}{48\pi^2} \alpha + \frac{-2m_z^2}{8\pi(4\pi)^2} \cdot \gamma,$$

where

$$\alpha = \left( \frac{1}{\epsilon^3} - \frac{1}{R_{\max}^3 + \epsilon^3} \right),$$

and

$$\gamma = \int \frac{9(\vec{n}_+ \vec{n}_- \cdot \vec{e}_z) n_+^z n_-^z - 3(\vec{n}_+^z)^2 - 3(\vec{n}_-^z)^2 + 1}{(r_+^3 + \epsilon^3)(r_-^3 + \epsilon^3)} dV.$$

## REFERENCES

Bertone S., Vogt C., Enßlin T., 2006, MNRAS, 370, 319

- Bonafede A., Govoni F., Murgia M., Feretti L., Dallacasa D., Giovannini G., Dolag K., Taylor G., 2008, in et al A. E., ed., Magnetic Fields in the Universe II The coma cluster magnetic field from faraday rotation measures. Rev. Mex. Astron. Astrof. (SC)
- Børve S., Omang M., Trulsen J., 2001, ApJ, 561, 82
- Brüggen M., Ruszkowski M., Simionescu A., Hoeft M., Dalla Vecchia C., 2005, ApJ, 631, L21
- Carilli C. L., Taylor G. B., 2002, ARA&A, 40, 319
- Cassano R., Brunetti G., Setti G., Govoni F., Dolag K., 2007, MNRAS, 378, 1565
- Chyzy K. T., Beck R., 2004, in Duc P.-A., Braine J., Brinks E., eds, Recycling Intergalactic and Interstellar Matter Vol. 217 of IAU Symposium, Magnetic Fields in Strongly Interacting Galaxy Systems. p. 436
- Clarke T. E., Kronberg P. P., Böhringer H., 2001, ApJ, 547, L111
- Daddi E., Dickinson M., Morrison G., Chary R., Cimatti A., Elbaz D., Frayer D., Renzini A., Pope A., Alexander D. M., Bauer F. E., Giavalisco M., Huynh M., Kurk J., Mignoli M., 2007, ApJ, 670, 156
- de Grijs R., 2001, ArXiv Astrophysics e-prints
- Dolag K., Bartelmann M., Lesch H., 1999, A&A, 348, 351
- Dolag K., Bartelmann M., Lesch H., 2002, A&A, 387, 383
- Dolag K., Borgani S., Murante G., Springel V., 2008, ArXiv e-prints
- Dolag K., Evrard A., Bartelmann M., 2001, A&A, 369, 36
- Dolag K., Grasso D., Springel V., Tkachev I., 2005, Journal of Cosmology and Astro-Particle Physics, 1, 9
- Dolag K., Meneghetti M., Moscardini L., Rasia E., Bonaldi A., 2006, MNRAS, 370, 656
- Dolag K., Reinecke M., Gheller C., Imboden S., 2008, ArXiv e-prints, 807
- Dolag K., Schindler S., Govoni F., Feretti L., 2001, A&A, 378, 777
- Dolag K., Staszczyn F. A., 2008, ArXiv e-prints, 807
- Dubois Y., Teyssier R., 2008, A&A, 482, L13
- Enßlin T. A., Biermann P. L., Kronberg P. P., Wu X.-P., 1997, ApJ, 477, 560
- Enßlin T. A., Vogt C., 2006, A&A, 453, 447
- Feretti L., Dallacasa D., Giovannini G., Tagliani A., 1995, A&A, 302, 680
- Feretti L., Dallacasa D., Govoni F., Giovannini G., Taylor G. B., Klein U., 1999, A&A, 344, 472
- Ferrari C., Govoni F., Schindler S., Bykov A. M., Rephaeli Y., 2008, Space Science Reviews, 134, 93
- Furlanetto S. R., Loeb A., 2001, ApJ, 556, 619
- Govoni F., 2006, Astronomische Nachrichten, 327, 539
- Govoni F., Feretti L., 2004, International Journal of Modern Physics D, 13, 1549
- Govoni F., Murgia M., Feretti L., Giovannini G., Dolag K., Taylor G. B., 2006, A&A, 460, 425
- Grasso D., Rubinstein H. R., 2001, Phys. Rept., 348, 163
- Guidetti D., Murgia M., Govoni F., Parma P., Gregorini L., de Ruiter H. R., Cameron R. A., Fanti R., 2008, A&A, 483, 699
- Hoffman Y., Ribak E., 1991, ApJ, 380, L5
- Johnston-Hollitt M., Ekers R. D., 2004, astro-ph/0411045
- Kim K.-T., Kronberg P. P., Tribble P. C., 1991, ApJ, 379, 80
- Klein U., Wielebinski R., Morsi H. W., 1988, A&A, 190, 41
- Kronberg P. P., 2006, Astronomische Nachrichten, 327, 517
- Kronberg P. P., Lesch H., Hopp U., 1999, ApJ, 511, 56
- Kulsrud R. M., Cen R., Ostriker J. P., Ryu D., 1997, ApJ, 480, 481
- Li S., Li H., Cen R., 2008, ApJS, 174, 1
- Mathis H., Lemson G., Springel V., Kauffmann G., White

- S. D. M., Eldar A., Dekel A., 2002, MNRAS, 333, 739  
Miniati F., Jones T. W., Kang H., Ryu D., 2001, ApJ, 562, 233  
Murgia M., Govoni F., Feretti L., Giovannini G., Dallacasa D.,  
Fanti R., Taylor G. B., Dolag K., 2004, A&A, 424, 429  
Reuter H.-P., Klein U., Lesch H., Wielebinski R., Kronberg P. P.,  
1994, A&A, 282, 724  
Ryu D., Kang H., Biermann P. L., 1998, A&A, 335, 19  
Ryu D., Kang H., Cho J., Das S., 2008, Science, 320, 909  
Saro A., Borgani S., Tornatore L., Dolag K., Murante G., Biviano  
A., Calura F., Charlot S., 2006, MNRAS, 373, 397  
Shu C.-G., Mo H.-J., Shu-DeMao 2005, Chinese Journal of As-  
tronomy and Astrophysics, 5, 327  
Sigl G., Miniati F., Enssblin T. A., 2004, Phys. Rev. D, 70, 043007  
Sofue Y., 1998, PASJ, 50, 227  
Soida M., Urbanik M., Beck R., Wielebinski R., Balkowski C.,  
2001, A&A, 378, 40  
Springel V., 2005, MNRAS, 364, 1105  
Springel V., Hernquist L., 2002, MNRAS, 333, 649  
Springel V., White S. D. M., Tormen G., Kauffmann G., 2001,  
MNRAS, 328, 726  
Subramanian K., Shukurov A., Haugen N. E. L., 2006, MNRAS,  
366, 1437  
Völk H. J., Atoyan A. M., 2000, ApJ, 541, 88  
Vogt C., Enßlin T. A., 2003, A&A, 412, 373  
Vogt C., Enßlin T. A., 2005, A&A, 434, 67